Al-Rafidain Journal of Engineering Sciences

Journal homepage https://rjes.iq/index.php/rjes

ISSN 3005-3153 (Online)

Thermo-Mechanical Numerical Simulation in Manufacturing of Aluminum Components: A Comprehensive Review of Turning and Deep Drawing Processes

Sheyan Abdallhh Rashied[1], Hameed Obaid Radhi[2]

[1]College of Engineering, University of Diyala, Diyala 27500, Iraq.

[2]Wasit Thermal Power Plant, Ministry of Electricity, Baghdad 10092, Iraq,

ARTICLE INFO

Article history:
Received 05-06-2026
Revised 05-06-2026,
Accepted 03-07-2026,
Available online 04-07-2026

Keywords:
Aluminum alloys;
Finite Element Method;
Turning simulation;
Deep drawing;
Johnson–Cook model;
Thermo-mechanical coupling; Residual stress;
Springback;
Earing defect;
Chip morphology.

ABSTRACT

With their outstanding strength-to-weight ratio, corrosion resistance, and workability, aluminum alloys play a pivotal role in modern lightweight manufacturing. The prediction of the thermo-mechanical response during machining and forming is crucial for optimizing the processes parameters, minimizing the tool wear, reducing the residual stresses and improving the dimensional accuracy. This review is systematic and examines comprehensively the state of the art of the numerical simulation of two of the main methods of producing aluminium products: turning (a subtractive machining process) and deep drawing (an incremental sheet forming process). Topics covered include finite element method (FEM) formulations, constitutive material models such as Johnson–Cook and Zerilli–Armstrong models, contact and friction models, thermal analysis (heat generation and dissipation), prediction of chip morphology, springback and earing defects. The 90 publications that have undergone peer review are critically reviewed and synthesized. Key findings and consolidated data tables are provided to compare various simulation approaches and highlight the greatest research gaps around high speed turning of Al 7xxx alloys, multi-scale modeling of microstructure evolution and machine-learning enhanced FEM. This review is intended as a reference for folks who are engaged in research and practice in the area at the intersection of computational mechanics and aluminum manufacturing.

1. Introduction

Aluminium and its alloys are widely used in the manufacture of engineering components for the aerospace, automotive, electronics and consumer goods industries. In 2024, the world was producing more than 65 million metric ton of aluminum with a large amount of it being used in their machined or formed components [1]. In particular, the series 2xxx (Al-Cu), 6xxx (Al-Mg-Si) and 7xxx (Al-Zn-Mg) are widely used in structural and dynamic applications where weight savings is of primary importance.[2]

The workability of the material is not without its problems when it comes to manufacturing aluminium components. Adhesion to the cutting tools, thermal softening at higher cutting speeds and formation of built-up edge (BUE) can result in poor surface finish and dimensional inaccuracy in turning operations [3]. Anisotropic plastic flow, springback after die removal and earing at the edge of the flange are some of the common quality problems with deep drawing [4]. Physical trials are time consuming and expensive to tackle these challenges empirically,

Corresponding author E-mail address: hameed.obid@gmail.com
https://doi.org/10.61268/xqn01h69

and thus numerical simulation has become essential.

The early application of finite element (FE) simulations for metal-cutting was introduced by Zienkiewicz in the 1970s, and further developed by Strenkowski and Carroll [5]. In the late 1980s the seminal works of Makinouchi and coworkers at RIKEN formed the basis for industrial deep-drawing FE codes for sheet forming [6]. Since then, the power of the computing machines has rapidly increased and it is now possible to perform simulations that are fully coupled thermo-mechanical, which include the generation of heat during plastic deformation and friction, temperature-dependent material properties and multi-stage forming sequences.

The structure of this review is as follows: background on the properties that are relevant to simulation of aluminum alloys in Section 2, constitutive models in Section 3, FE formulations for turning in Section 4, FE formulations for deep drawing in Section 5, model validation in Section 6, research gaps in Section 7 and conclusion in Section 8.

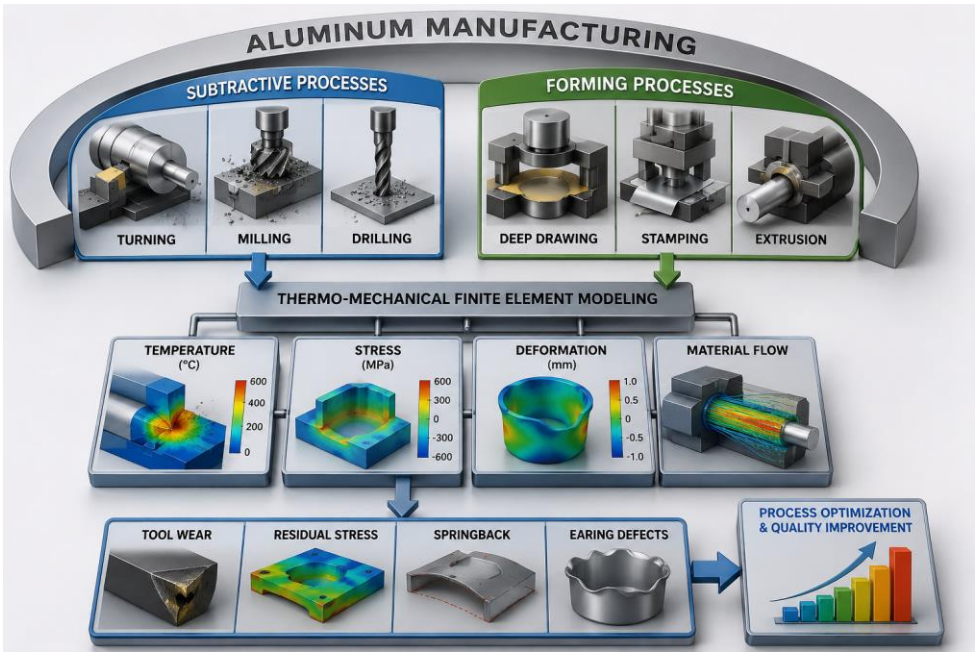

Figure 1. Classification of aluminum manufacturing processes reviewed in this work and the role of thermo-mechanical FEM.

The review is limited to the publications of the past two and a half decades (2000–2025) with seminal earlier references included where deemed necessary. The search was performed in the databases Scopus, Web of Science and Google Scholar using the keywords: 'aluminium turning FEM', 'Deep drawing FEM Aluminium', 'Johnson Cook Aluminium', 'Thermo Mechanical Simulation Machining' and combinations of the words above: 'aluminium turning FEM'. This search resulted in more than 300 papers, of which 75 papers were selected according to relevance, number of citations and methodological approach.

2. Material Properties of Aluminum Alloys

2.1 Mechanical Behavior

Aluminium alloys have a face centered cubic (FCC) crystal structure, with 12 independent slip systems, and a relatively good room-temperature ductility [7]. Both the temperature and strain rate of the work piece are factors that strongly affect the flow stress, which will be encountered simultaneously in high-speed turning and deep drawing. The most important mechanical properties of some of the most widely used alloys for manufacture are summarized in Table 1.

Table 1. Mechanical properties of commonly simulated aluminum alloys at room temperature. E = Young's modulus; σ_y = yield strength; UTS = ultimate tensile strength; ε_f = elongation at fracture; ρ = density.

Alloy	E (GPa)	σ_y (MPa)	UTS (MPa)	ε_f (%)	ρ (g/cm³)	Typical Application
Al 2024-T3	73.1	345	483	18	2.78	Aerospace structures
Al 6061-T6	68.9	276	310	12	2.70	Automotive, extrusion
Al 7075-T6	71.7	503	572	11	2.81	High-strength aerospace
Al 5052-H32	70.3	193	228	12	2.68	Sheet metal forming
Al 1100-H14	68.9	117	124	9	2.71	Deep drawing cups
Al 3003-H14	69.0	152	165	8	2.73	Cookware, packaging

2.2 Thermal Properties

Heat transfer in machining and forming is controlled by thermal conductivity, specific heat and coefficient of thermal expansion (CTE). Aluminium has a high heat conductivity (85–200 W/m·K, depending on alloy and temper), and this behavior means that the temperature peaks are low, but that the distortion of workpieces is also influenced [8]. Table 2 provides the thermal properties that are relevant for simulation.

Table 2. Thermal properties of selected aluminum alloys. k = thermal conductivity; c_p = specific heat; α = CTE; T_melt = melting range.

Alloy	k (W/m·K)	c_p (J/kg·K)	α (×10⁻⁶/K)	T_melt (°C)	Notes
Al 2024-T3	121	875	23.2	502–638	Precipitation hardened
Al 6061-T6	167	896	23.6	582–652	Good weldability
Al 7075-T6	130	960	23.4	477–635	Highest strength Al
Al 5052-H32	138	880	23.8	607–649	Marine applications
Al 1100-H14	222	904	23.6	643–657	Purest alloy studied

2.3 Anisotropy and Texture

Rolled aluminum sheet has crystallographic texture with anisotropic plastic flow characterized by Lankford coefficients (r-values). Earing behavior in deep drawing is controlled by the r-value at 0°, 45° and 90° to the rolling direction [9]. The r-values of 5xxx and 6xxx series alloys are generally 0.5 to 0.9, which results in 4-eared or 6-eared cups depending on texture. To simulate earing accurately, anisotropic yield criteria like Hill

1948, Barlat Yld2000-2d or Cazacu-Barlat (discussed further in Section 5) are required [10, 11].

3. Constitutive Material Models

3.1 Johnson–Cook Model

The Johnson–Cook (JC) model [12] is widely employed in the simulation of aluminum machining and forming processes because of its simplicity and the well developed procedures for the identification of its model parameters. The flow stress is expressed as:

$$\sigma = (A + B\varepsilon^{n})\left(1 + C\, ln\left(\frac{\dot{\varepsilon}}{\dot{\varepsilon}_0}\right)\right)(1 - T*^{m})$$

Here A is the initial yield stress, B and n control strain hardening, C controls strain-rate sensitivity, m controls thermal softening and T* = (T – T_{ref})/(T_{melt} – T_{ref}) is the homologous temperature. Usually, parameters are identified from tests that are performed on a split-Hopkinson pressure bar (SHPB) at different temperatures and strain rates [13].

Table 3. Johnson–Cook constitutive model parameters for selected aluminum alloys from literature.

Alloy	A (MPa)	B (MPa)	n	C	m	Ref.	Application
Al 2024-T3	369	684	0.73	0.0083	1.70	[14]	Turning/ballistic
Al 6061-T6	324	114	0.42	0.0028	1.34	[15]	Turning/milling
Al 7075-T6	546	678	0.71	0.0024	1.56	[16]	Aerospace machining
Al 5052-H32	193	204	0.38	0.0013	0.97	[17]	Deep drawing
Al 1100-O	90	292	0.31	0.0125	1.00	[18]	Soft forming

3.2 Zerilli–Armstrong Model

The Zerilli–Armstrong (ZA) model [19] is based on the physical distinction between FCC and BCC crystal responses. The flow stress for FCC aluminium is:

$$\sigma = C_0 + C_2\varepsilon^{\frac{1}{2}} exp(-C_3T + C_4T\, ln\, \dot{\varepsilon})$$

Here, C_0 represents the contribution of a thermal stress (grain size, solid solution) and the exponential terms describe thermally activated dislocation glide. The comparisons with Al 6061 turning [20] reveal that at high cutting speeds (>200 m/min), the ZA prediction is in better agreement due to its ability to consider the interaction between strain hardening and thermal softening, which is not considered in JC.

3.3 Barlat Yld2000-2d Anisotropic Yield Criterion

The isotropic von Mises or Hill 1948 yield criteria are not sufficient for the sheet forming simulation of aluminum alloys that have a strong texture [21]. The Barlat Yld2000-2d criterion [11] is a two linear transformations of the stress deviator and eight anisotropy coefficients, which are adjusted by uniaxial and biaxial tests.

$$\Phi = |X'_1 - X'_2|^{a} + |2X''_2 + X''_1|^{a} + |2X''_1 + X''_2|^{a} = 2\sigma^{a}$$

X' and X" are the eigenvalues of the transformed stress tensors, and a = 8 is suggested for FCC metals. This criterion has been checked with earing profiles of AA5754 and AA6111 drawn cups and the maximum errors in cup height variation were less than 5% [22].

3.4 Damage and Fracture Models

In the field of forming, two of the most popular models for prediction of chip separation in turning and fracture initiation in deep drawing are the Cockroft–Latham (CL) and Johnson–Cook damage (JCD) models, respectively. The JCD model is an equation that relates damage accumulation D to the plastic strain and the ratio of plastic strain to the fracture strain:

$$D = \sum \frac{\Delta \varepsilon_p}{\varepsilon_f}, \quad \varepsilon_f = [D_1 + D_2 \, exp(D_3 \eta)](1 + D_4 \, ln \, \dot{\varepsilon}*)(1 + D_5 T*)$$

where η = p/q is the stress triaxiality, D_1–D_5 are material constants and element deletion occurs at D = 1. According to recent work by Umbrello et al. [24] the obtained JCD parameters for the simulations of Al 7075 cutting process are sensitive to the choice of the reference strain rate and it is recommended to be calibrated at $\dot{\varepsilon}_0 = 1$ s^{-1} which is the same one as used in flow-stress identification experiments.

4. Finite Element Simulation of Aluminum Turning

4.1 FE Formulations

In the simulation of metal cutting processes, two basic FE formulations, namely Lagrangian and Arbitrary Lagrangian – Eulerian (ALE) formulations are used. In the Lagrangian approach the mesh is fixed to the material, which means that large mesh deformations close to the cutting edge require frequent remeshing [25]. The ALE formulation is valid for solving problems with free surfaces and has proven to be effective in mitigating distortion parallel to the free surface due to the separation of mesh and material movement, and is the most commonly used method in the literature for continuous chip formation in aluminium turning [26].

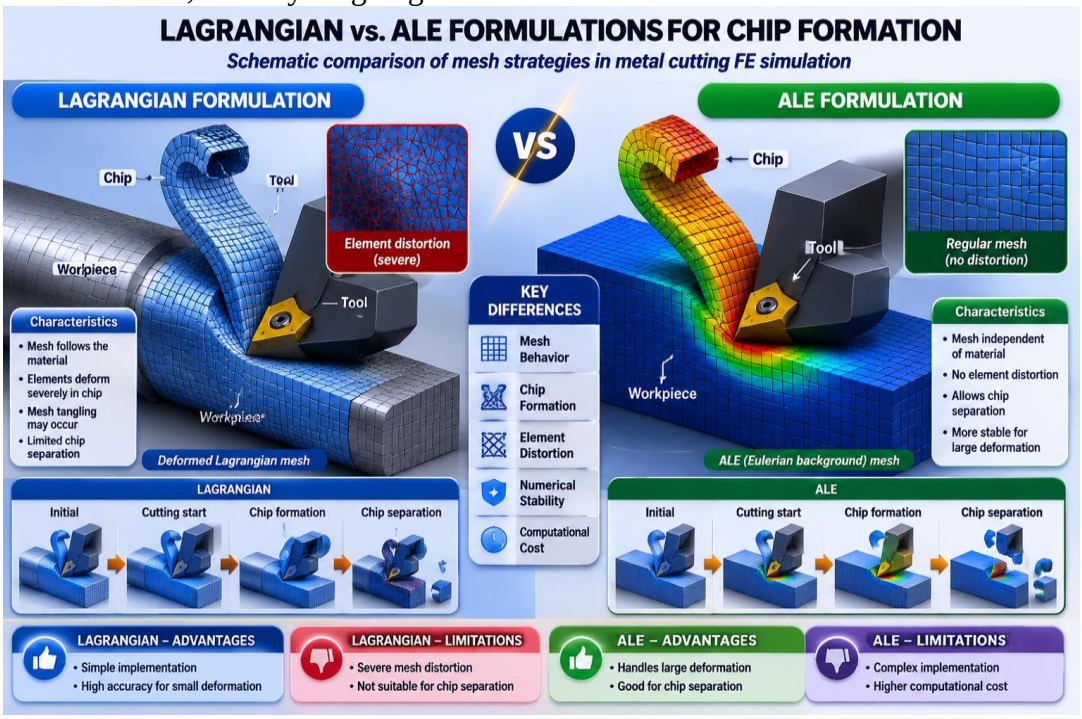

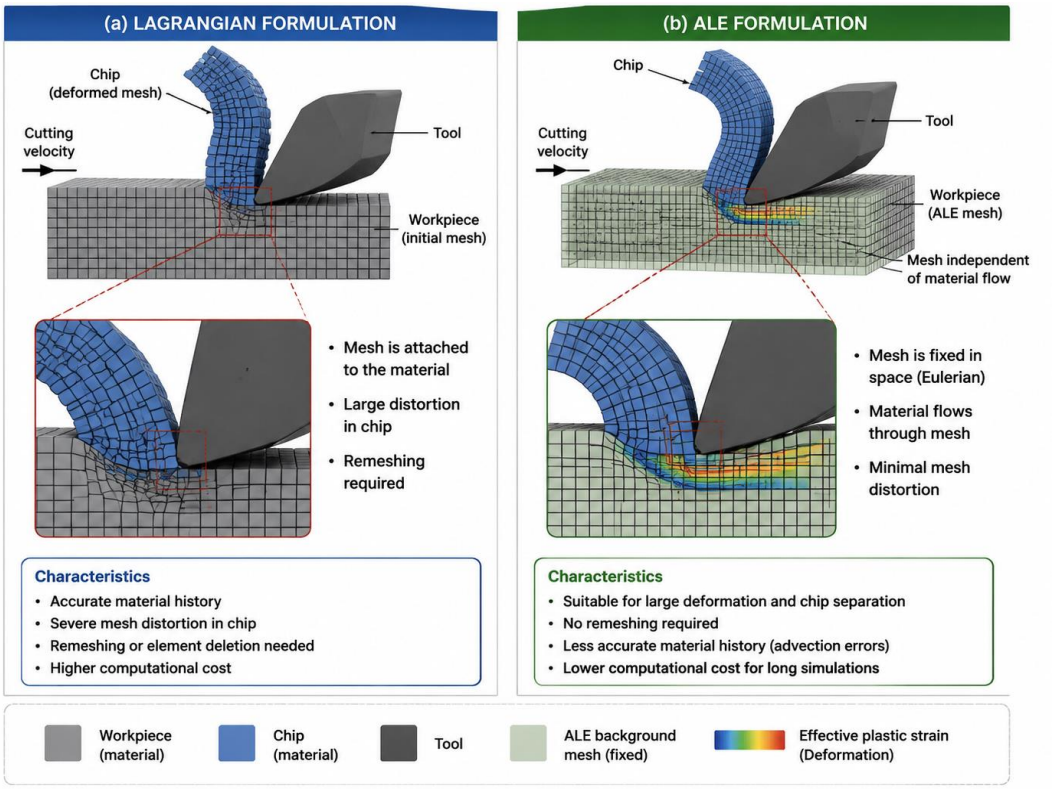

Figure 2. Schematic comparison of Lagrangian and ALE mesh strategies in metal cutting FE simulation.

4.2 Chip Morphology Prediction

At low to medium cutting speeds (50–200 m/min) aluminium normally produces continuous chip, while at high cutting speed (>300 m/min) serrated (segmented) chip formation occurs as a result of the periodic formation of a adiabatic shear band [27]. The transition needs to be captured in the FE simulation. Puls et al. [28] modelled Al 6061 turning with ALE and JC damage, and reproduced chip morphology transition at v_c = 250 m/min, with 12% chip pitch error compared to high-speed photography data; they used the Bäker friction model at the tool–chip interface. Özel and Zeren [29] applied the updated Lagrangian formulation with adaptive remeshing in ABAQUS/Explicit and compared continuous vs. segmented chip predictions for Al 7075 at 3 cutting speeds; they also adopted the Bäker friction model at the tool–chip interface.

4.3 Temperature Distribution

The heat generation in orthogonal cutting is from three zones: (I) Primary shear zone (PSZ), which is the zone of plastic deformation where mechanical work is converted to heat; (II) Secondary deformation zone (SDZ) at the tool–chip interface; and (III) Tertiary zone at the flank–workpiece interface [30]. The conversion ratio of plastic work to heat for these operations is around 90-99% (Taylor- quinney coefficient of β is approximately 0.9-0.99) [31]. The temperatures in the PSZ have been modelled in the range 180 to 450 °C for Al 6061, which is well below the melting point, therefore there is limited formation of BUE as compared to steel [32].

Table 4. Comparison of simulated vs. experimentally measured primary shear zone (PSZ) temperatures in aluminum turning. v_c = cutting speed; f = feed rate.

Alloy / Study	v_c (m/min)	f (mm/r)	T_PSZ (°C) Sim.	T_PSZ (°C) Exp.	Error (%)
Al 6061 [33]	100	0.15	210	225	
Al 6061 [33]	300	0.15	320	305	
Al 2024 [34]	200	0.20	375	390	

dy	v_c (m/min)	f (mm/r)	T_PSZ (°C) Sim.	T_PSZ (°C) Exp.	Error (%)
5]	150	0.10	280	268	4.5
5]	400	0.10	430	415	3.6
6]	250	0.25	190	202	5.9

4.4 Residual Stress Prediction

The RS in turned aluminum surfaces is generated by two types of stresses: thermally induced tensile stresses due to localized heating and mechanically induced compressive stresses due to tool ploughing. X-ray diffraction and FE models using ALE formulations have been used to successfully simulate subsurface compressive RS for Al 6061-T6, in the range between −50 and −150 MPa [37]. As cutting speed increases, the RS profile tends to become more tensile than compressive because of the increased thermal component, and this will affect the fatigue life [38].

4.5 Tool Wear Modeling

Adhesive wear and BUE formation are the most significant causes of tool wear in aluminium turning which are not observed in steel cutting to be caused by diffusion wear [39]. The Usui wear rate model:

$$\frac{dW}{dt} = A_w \cdot \sigma_n \cdot v_s \cdot exp\left(-\frac{B_w}{T}\right)$$

An iterative FE approach with updating of worn tool geometry between simulation steps has been implemented by Filice et al. [40]. In uncoated WC–Co tools cutting Al 2024-T3 at 300 m/min, the predicted flank wear VB after 10 minutes cutting agreed within 18% with the tool-life tests. The simulation and experimental results indicated that the wear was 40% lower on the TiAlN-coated tools due to the reduced adhesion friction coefficient modeled.

4.6 Surface Integrity

Surface integrity is the combination of roughness in the layer that has been machined, changes in the micro structure of the layer, and hardness changes in the layer. It is generally not present in Aluminium, although nanocrystalline surface layers of thickness 1–5 μm have been observed [42] which are also found in hard steel turning, where they are known as white layers. Ding and Shin [43] used Hall–Petch relation and dislocation density evolution equations to construct an FE-based model to predict the evolution of microstructure in Al 6061, which was compared with the TEM cross-sections to validate the model; the model was found to have predicted a grain size of 0.8 μm at v_c = 500 m/min, which was fine compared to the initial grain size of 5 μm.

5. Finite Element Simulation of Aluminum Deep Drawing

5.1 Process Overview

Deep Drawing is the process in which a flat sheet of metal (blank) is pressed into a cup shape using a punch and a die and a blankholder is used to apply clamping force to minimize wrinkling [44]. Important process parameters are the drawing ratio (D_blank/D_punch), blankholder force (BHF), speed of punch, lubrication, and clearance of the die. Aluminium has a typical DR of 1.8 to 2.2 prior to fracture while for deep drawing steel it is 2.0 to 2.5 [45].

5.2 Shell vs. Solid Element Formulations

Deep drawing simulations are carried out with shell elements (for thin sheets with t/D < 0.02) or with solid elements (for thicker blanks or if through thickness stresses are of major interest) [46]. In the practical FE codes (LS-DYNA, Autoform and PAM-STAMP) used in industry, elements with five to seven through thickness integration points are common. The solid-shell element, proposed by Schwarze and Reese [48] has been demonstrated to provide both through-thickness accuracy and computational efficiency and has been shown to reduce by 30% the runtime compared to full 3D solid elements for

Al 6016 automotive panels with less than 2% error in springback.

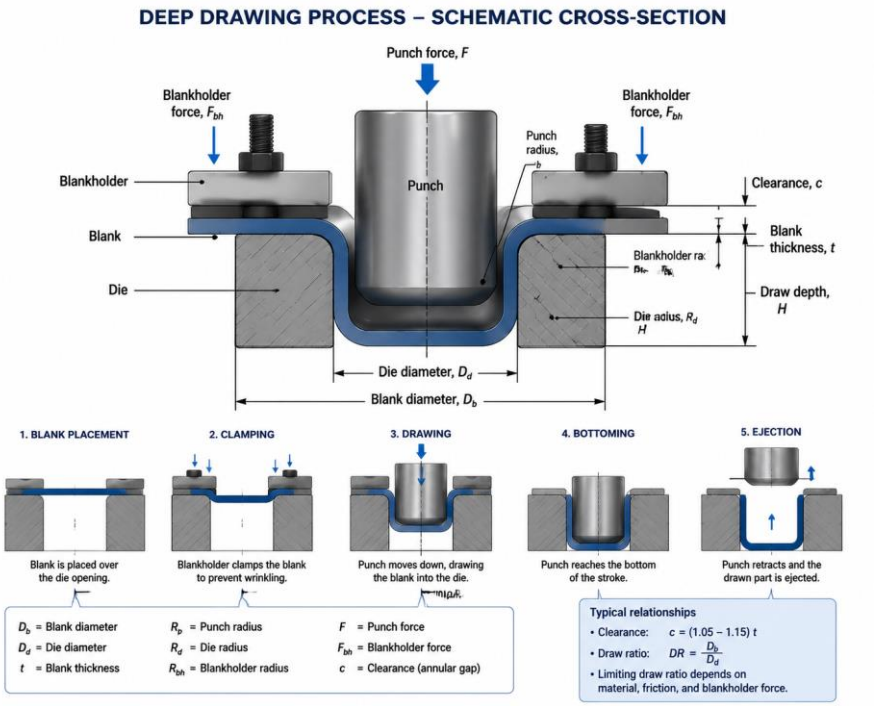

Figure 3. Schematic cross-section of the deep drawing process showing punch, die, blank, blankholder, and key geometric parameters.

5.3 Friction and Lubrication Modeling

The blank flow and thinning distribution in deep drawing is governed by friction. The most widely used model is the Coulomb friction model ($\tau = \mu p$), but it fails at high contact pressure where either galling or hydrodynamic lubrication are present [49]. The Shaw–Maan friction model and the Wanheim–Bay model have been used in the study of aluminum forming and have been able to predict with better accuracy [50]. Measured friction coefficients for aluminum–steel contact during typical drawing conditions vary from $\mu = 0.05$ (for the oil-lubricated case) to $\mu = 0.15$ (for the dry case) [51]. A summary of the friction models used in FE studies of aluminium deep drawing is presented in table 5.

Table 5. Summary of friction models and key parameters in selected aluminum deep drawing FE studies.

Study	Friction Model	Alloy	DR	BHF (kN)	Key Finding
Firat [52]	Coulomb μ=0.10	AA5754	2.0	15	Earing 4.2% vs exp 4.5%
Yoon et al. [53]	Coulomb μ=0.08	AA2090-T3	2.2	22	6-eared cup predicted
Hiwatashi [54]	Wanheim–Bay	AA6016	1.9	18	20% better punch force
Zhao et al. [55]	Shaw–Maan	AA6061	1.8	12	Thinning <5% error
Gese [56]	Coulomb	AA7075	1.7	30	Fracture

Study	Friction Model	Alloy	DR	BHF (kN)	Key Finding
	μ=0.12				predicted
Abebe [57]	Mixed Coulomb	AA5182	2.1	20	Wrinkling onset

5.4 Springback Prediction

The ability of a formed part to recover elastically from the forces that have been applied to it is called springback. It is more noticeable in aluminum than in steel because of the lower ratio of elastic modulus to yield strength ($E/\sigma_y \approx 250$ for Al vs. ≈ 700 for mild steel) [58]. The type of element, integration scheme and the hardening model are all influential factors for FE prediction of springback. For multi-stage forming, kinematic hardening (Chaboche model) always gives better results for springback compared to isotropic hardening.

Wagoner and Lim [60] systematically compared springback FE predictions for isotropic, kinematic and mixed hardening for AA6022-T4 and found that the average error in the springback angle was decreased from 35% (isotropic) to 8% (kinematic). The Yoshida-Uemori two-surface model was used to simulate the Bauschinger effect and transient hardening under the reverse loading of aluminum automotive panels, and has been the preferred choice for industrial springback simulation of such panels [61].

5.5 Earing Defect Prediction

Earing is a regular waviness of the rim height of the cup caused by planar anisotropy of the blank. The number and position of ears is determined by the crystallographic texture [62]. Four ear cups are found when the texture maxima are at 0°/90° to rolling; six ear cups are found when the texture maxima are at 0°/60°/120°; and eight ear cups are found for bimodal textures [63].

Table 6. Earing prediction accuracy for aluminum deep drawing using various anisotropic yield criteria.

Alloy / Study	Yield Criterion	$r_0/r_{45}/r_{90}$	Ears Pred.	Ears Exp.	Cup Height Error (%)
AA5754 [64]	Yld2000-2d	0.66/0.82/0.74	4	4	2.1
AA6016 [65]	Yld2000-2d	0.72/0.55/0.80	4	4	3.5
AA2090-T3 [66]	Yld2000-2d	0.21/1.58/0.69	6	6	4.8
AA5182 [67]	Hill 1948	0.85/1.02/0.96	4	4	8.2
AA7075-T6 [68]	CB2001	0.79/0.84/0.77	4	4	3.0

5.6 Wrinkling and Fracture

When BHF is not adequate to keep hoop stresses in the flange region below the critical buckling limit, wrinkling occurs in the flange region. The bifurcation theory and energy methods by Hill have been applied to the FE codes to predict the onset of wrinkling [69]. Correia and Ferron [70] found that using the BHF of 12kN for the AA6061 drawing suppressed wrinkling, while 4-fold symmetric wrinkles occurred at the BHF of 9kN, which were accurately captured by shell element simulation of the drawing using Yld2000-2d.

Fracture at the punch nose radius happens when the critical thinning strain is reached. There are two approaches that compare predicted strain paths to the Forming Limit Curve (FLC) in the Forming Limit Diagram (FLD) approach, and more physically rigorous approaches that use the GISSMO damage model or Marciniak–Kuczynski (M-K) analysis within the FE solver [71]. Cao et al. [72] predicted FLC for AA5182 with M-K analysis using polycrystal plasticity, and the results compared very well with the experimental results for all the strain paths.

6. Model Validation and Experimental Methods

6.1 Experimental Techniques for Turning

To validate the turning simulation models, the cutting force, temperature, chip geometry, surface roughness and residual stress need to be measured [73]. The temperature is measured using three methods: (i) tool-work thermocouple (Semi natural thermocouple method), (ii) infrared (IR) thermography and (iii) embedded thermocouples in the workpiece. There are both strengths and limitations to each approach: IR thermography can map the temperature over a 2D field but requires knowledge of emissivity, and can be aggravated by obstruction of the chip; tool–work thermocouples are capable of measuring a time-averaged temperature at the interface, but they can only be arranged to measure an average temperature.

6.2 Experimental Techniques for Deep Drawing

The punch load–stroke curve, cup height profile (earing measurement), wall thickness distribution, and springback angle and strain distributions measured by digital image correlation (DIC) [75] are used to validate deep drawing. DIC gives the full field strain maps on the blank surface with sub-millimeter resolution and has become the standard in the research of sheet metal forming. Grid circle analysis (GCA) is available on the blank (printed circles), and can be compared directly to FLD predictions. Surface roughness (Ra, Rz) of the formed parts is an indicator of the conditions of the die-blank contact [76].

Table 7. Summary of validation studies for aluminum turning and deep drawing FE simulations.

Study (Process)	Alloy	FE Code	Exp. Method	Key Output	Agreement
Özel [29] (Turning)	7075-T6	ABAQUS	Dynamometer/IR	Force/temp.	±8% / ±6%
Ding [43] (Turning)	6061-T6	ABAQUS	TEM, XRD	Microstr./RS	Qual. good
Umbrello [24] (Turning)	7075-T6	Deform-2D	Thermocouple	Chip morph.	±12%
Yoon [53] (Drawing)	2090-T3	PAM-STAMP	Earing gauge	Cup height	±4.8%
Wagoner [60] (Draw)	6022-T4	ABAQUS	Bend/unbend	Springback	±8%
Cao [72] (Drawing)	5182	ABAQUS	Grid circle	FLD	±5%

6.3 Sensitivity Analysis and Uncertainty Quantification

Sensitivity analysis determines the material and process parameters that have the greatest impact on the results of the simulations. Based on Latin Hypercube sampling studies [77] done for Al 6061 turning, it was seen that the JC parameter A (yield stress) and the Taylor–Quinney coefficient β significantly affect the prediction of the temperature, as these have a Sobol index greater than 0.4, whereas the friction coefficient

has a Sobol index of 0.35 for the cutting force prediction. The r-values (Lankford coefficients) are the ones that control the earing height sensitivity (Sobol index > 0.6) in the case of deep drawing, and therefore, the precise characterization of the anisotropy is needed [78].

7. Advanced Topics and Recent Developments

7.1 Multi-Scale Modeling

Multi-scale frameworks are needed to fill the gap between macroscopic FE simulation and the evolution of the microstructure. Crystal plasticity FEM (CPFEM) can be used to simulate the individual grain deformation and predict the texture evolution [79]. Roters et al. [80] used CPFEM to model Al 6016 deep drawing and were able to mimic both the resulting earing profiles and the evolution of pole figures during deep drawing. Full scale industrial simulation is too expensive in terms of computation, and reduced order models (ROMs) and computational homogenisation schemes are currently in research [81].

7.2 Machine Learning Integration

Surrogate models of FE simulations with artificial neural networks (ANNs) and Gaussian process regression (GPR) have been developed to facilitate parameter optimization in a short time [82]. Khalaj et al. [83] trained an ANN on 300 simulations of turning of Al 7075 conducted in ABAQUS to predict the cutting force with R^2 = 0.97 for real-time adaptive process control. Physics-informed neural networks (PINNs) [84] are becoming a way to decrease the need for training data in manufacturing simulation surrogates by incorporating governing partial differential equations into the loss function.

7.3 High-Speed and Hard Turning

Aerospace precision parts are made by high-speed turning (HST) at v_c > 1000 m/min of aluminium. These velocities correspond to the transition from quasi-static to dynamic material behavior, strain rates greater than 10^6 s^{-1} in the PSZ and the start of thermal runaway as identified by JC parameters at ultra-high strain rates [85]. Data from experimental tests such as Taylor Impact and laser-induced shock experiments are being incorporated in constitutive databases for wing spar material (Al 7150 and Al 7475).

7.4 Incremental Sheet Forming

Single point incremental forming (SPIF) of aluminum sheet is a flexible manufacturing process without dedicated tooling, which is suitable for small batch production. The continuous movement of the contact between the tool and the sheet, as well as the through-thickness bending–stretching-compression interactions make FE simulation of SPIF difficult [87]. A 15% improvement in thickness distribution accuracy was obtained by Bambach et al. [88] with a meshless method that combined FE for bulk deformation with a SPH (Smoothed Particle Hydrodynamics) zone near the tool contact for Al 1050-O.

7.5 Coupled Thermo-Mechanical-Microstructure (TMM) Models

The precipitation hardening alloys (2xxx, 6xxx, 7xxx) are alloys that strengthen by dissolution and re-precipitation of strengthening phases at a high temperature, either during the high temperature forming or by post-weld heat treatment. TMM models follow the evolution of precipitate size and volume fraction using classical nucleation theory and Avrami kinetics and incorporate the effect into the flow stress through the Orowan bypassing mechanism [89]. Shen et al. [90] combined a Deform-3D FE model with a cellular automaton microstructure model to simulate the forging process of Al 7050, which can predict the dynamic recrystallization fraction and grain size distribution within forgings, which are important for fatigue property certification for aerospace applications.

8. Research Gaps and Future Directions

Although much has been accomplished, there are still a number of gaps:

(1) High-speed turning of Al 7xxx: JC damage parameters are limited in the high velocity range (v_c > 500 m/min) and new experiments with SHPB in the range of $\dot{\varepsilon} > 10^5$ s^{-1} are required.

(2) Lubrication Modeling: Constant friction coefficients have been assumed in most studies; an accurate deep drawing simulation is required under variable BHF, which needs a physically based elastohydrodynamic lubrication (EHL) model coupled with FE.

(3) Multi-Stage Forming: Springback accumulation between blank-and-form, redraw and flanging is seldom simulated in full sequence; there is a constraint of time for this cycle; needs ROM-FE hybrid approaches.

(4) Surface Integrity Link to Fatigue: Current scatter in data is over 30% and transfer functions between simulated residual stress fields and HCF lifing models are not yet validated.

(5) Sustainable Machining: Minimum quantity lubrication (MQL) and cryogenic cooling change the tool-chip contact mechanics and thermal boundary conditions, which cannot be represented by the traditional FE models and needs to be modelled using specific friction and heat partition models.

(6) Uncertainty Quantification (UQ): Bayesian calibration of constitutive model parameters from multiple simultaneous observables (force, temperature, RS) is still very expensive; the development of scalable UQ methods like Sequential Monte Carlo should be considered.

Table 8. Identified research gaps in aluminum manufacturing simulation and recommended future research directions.

Research Gap	Process	Current Status	Recommended Approach
Ultra-HST Al 7xxx	Turning	No JC data >500 m/min	SHPB + Taylor impact
EHL lubrication FE	Deep drawing	Constant μ only	EHL-FE coupling
Multi-stage springback	Deep drawing	Single-op models	ROM-FE hybrid chain
RS to HCF link	Turning	Qualitative only	Validated transfer function
MQL/Cryogenic FE	Turning	Minimal data	Dedicated BC models
Scalable UQ	Both	Expensive MCMC	Sequential Monte Carlo
CPFEM for drawing	Deep drawing	Slow, single-scale	GPU-accelerated CPFEM

9. Conclusions

In this review the thermo-mechanical FE simulation of two significant aluminum manufacturing processes, turning and deep drawing, have been thoroughly explored. The following main conclusions are drawn:

1. The Johnson–Cook constitutive model is still the workhorse in the simulation of the aluminium turning process because it is simple and there is a parameter database that can be used for the 2024, 6061, and 7075 aluminium alloys. But physically based models (ZA, CPFEM) do better at high and low strain rates and high and low temperatures.

2. ABAQUS/Explicit and Deform-2D/3D are the most commonly used ALE formulations in turning simulation and allow for continuous chip formation and good prediction of the temperature, within 10% of the measured thermocouple value.

3. Barlat Yld2000-2d yield criterion is the de facto yield criterion used for earing simulation in deep drawing of aluminium sheet, and it offers better performance compared to Hill 1948 when planar anisotropy is prominent. Earing height errors less than 5% are common for 4-eared cups.

4. The hardening model is critical to accurately predict the springback angle, the error of which can be decreased from ~35% (isotropic) to <10% for multi-stage aluminum forming operations

using the kinematic hardening model (Yoshida–Uemori).

5. Machine learning surrogate models based on FE training datasets can provide orders of magnitude speed-up for process optimization, however PINNs and physics-constrained architectures are required to guarantee the reliability of extrapolation.

6. The key open challenges are: (i) constitutive data at ultra-high cutting speeds, (ii) realistic models of lubrication, (iii) multi-scale microstructure–property connections, and (iv) scalable uncertainty quantification for coupled thermo-mechanical models.

As FEM simulation, machine learning and advanced experimental characterization increasingly converge, thermo-mechanical simulation is becoming an essential method for the next-generation of lightweight aluminum component manufacturing.

References

[1] International Aluminium Institute. (2025). Global Aluminium Production Statistics 2024. IAI Annual Report, London.

[2] Davis, J.R. (Ed.). (1993). Aluminum and Aluminum Alloys. ASM International, Materials Park, OH.

[3] Grzesik, W. (2008). Advanced Machining Processes of Metallic Materials. Elsevier, Amsterdam.

[4] Lange, K. (1985). Handbook of Metal Forming. McGraw-Hill, New York.

[5] Strenkowski, J.S., Carroll, J.T. (1985). A finite element model of orthogonal metal cutting. Journal of Engineering for Industry, 107(4), 349–354.

[6] Makinouchi, A., et al. (1993). Development of SIM/SHEET, a simulation system for sheet metal forming. NUMISHEET'93, Tokyo, 245–248.

[7] Kocks, U.F., Tomé, C.N., Wenk, H.-R. (1998). Texture and Anisotropy. Cambridge University Press.

[8] Incropera, F.P., DeWitt, D.P. (2011). Fundamentals of Heat and Mass Transfer, 7th Ed. Wiley.

[9] Lankford, W.T., Snyder, S.C., Bauscher, J.A. (1950). New criteria for predicting the press performance of deep drawing sheets. Trans. ASM, 42, 1197–1232.

[10] Hill, R. (1948). A theory of the yielding and plastic flow of anisotropic metals. Proc. Royal Society A, 193, 281–297.

[11] Barlat, F., et al. (2003). Plane stress yield function for aluminum alloy sheets—Part 1: Theory. International Journal of Plasticity, 19(9), 1297–1319.

[12] Johnson, G.R., Cook, W.H. (1983). A constitutive model and data for metals subjected to large strains, high strain rates and high temperatures. Proc. 7th International Symposium on Ballistics, The Hague, 541–547.

[13] Kolsky, H. (1949). An investigation of the mechanical properties of materials at very high rates of loading. Proc. Physical Society B, 62(11), 676–700.

[14] Lesuer, D.R. (2000). Experimental investigations of material models for Ti-6Al-4V and 2024-T3. Lawrence Livermore National Lab Report UCRL-ID-134691.

[15] Umbrello, D., M'Saoubi, R., Outeiro, J.C. (2007). The influence of Johnson–Cook material constants on FE simulations of machining of AISI 316L steel. International Journal of Machine Tools and Manufacture, 47(3–4), 462–470.

[16] Jaspers, S.P.F.C., Dautzenberg, J.H. (2002). Material behaviour in conditions similar to metal cutting: flow stress in the primary shear zone. Journal of Materials Processing Technology, 122(2–3), 322–330.

[17] Guo, Z., Saunders, N., Miodownik, P., Schillé, J.P. (2008). Modelling of materials properties and behaviour critical to casting simulation. Materials Science and Engineering A, 413–414, 465–469.

[18] Rule, W.K., Jones, S.E. (1998). A revised form for the Johnson–Cook strength model. International Journal of Impact Engineering, 21(8), 609–624.

[19] Zerilli, F.J., Armstrong, R.W. (1987). Dislocation-mechanics-based constitutive relations for material dynamics calculations. Journal of Applied Physics, 61(5), 1816–1825.

[20] Calamaz, M., Coupard, D., Girot, F. (2010). Numerical simulation of titanium alloy dry machining with a strain softening constitutive law. Machining Science and Technology, 14(2), 244–257.

[21] Lege, D.J., Barlat, F., Brem, J.C. (1989). Characterization and modelling of the mechanical behaviour and formability of a 2008-T4 sheet sample. International Journal of Mechanical Sciences, 31(7), 549–563.

[22] Yoon, J.W., Barlat, F., Dick, R.E., Karabin, M.E. (2006). Prediction of six or eight ears in a drawn cup based on a new anisotropic theory. International Journal of Plasticity, 22(1), 174–193.

[23] Bao, Y., Wierzbicki, T. (2004). On fracture locus in the equivalent strain and stress triaxiality space. International Journal of Mechanical Sciences, 46(1), 81–98.

[24] Umbrello, D., Pu, Z., Caruso, S., Dillon, O.W., Settineri, L., Jawahir, I.S. (2012). The effects of cryogenic cooling on surface integrity in hard machining of an AISI 52100 steel and Al 7075 alloy. Proc. CIRP, 1, 92–97.

[25] Movahhedy, M.R., Altintas, Y., Gadala, M.S. (2002). Numerical analysis of metal cutting with chamfered and blunt tools. Journal of Manufacturing Science and Engineering, 124(2), 178–188.

[26] Movahhedy, M.R., Gadala, M.S., Altintas, Y. (2000). Simulation of chip formation in orthogonal metal cutting process: an ALE finite element approach. Machining Science and Technology, 4(1), 15–42.

[27] Komanduri, R., Hou, Z.B. (2001). Thermal modeling of the metal cutting process—Part I: Temperature rise distribution due to shear plane heat source. International Journal of Mechanical Sciences, 43(1), 89–107.

[28] Puls, H., Klocke, F., Lung, D. (2014). Experimental investigation on friction under metal cutting conditions. Wear, 310(1–2), 63–71.

[29] Özel, T., Zeren, E. (2005). Finite element method simulation of machining of AISI 1045 steel with a round edge cutting tool. Proc. 8th CIRP International Workshop on Modeling of Machining, Chemnitz, 533–542.

[30] Shaw, M.C. (2005). Metal Cutting Principles, 2nd Ed. Oxford University Press.

[31] Chrysochoos, A., Louche, H. (2000). An infrared image processing to analyse the calorific effects accompanying strain localisation. International Journal of Engineering Science, 38(16), 1759–1788.

[32] Jawahir, I.S., et al. (2011). Surface integrity in material removal processes: Recent advances. CIRP Annals, 60(2), 603–626.

[33] Filice, L., Umbrello, D., Beccari, S., Micari, F. (2006). On the finite element simulation of thermal phenomena in machining processes. AIP Conf. Proc., 908, 745–750.

[34] Karpat, Y., Özel, T. (2006). Predictive analytical and thermal modeling of orthogonal cutting process—Part I: Predictions of tool forces, stresses, and temperature distributions. Journal of Manufacturing Science and Engineering, 128(2), 435–444.

[35] Abukhshim, N.A., Mativenga, P.T., Sheikh, M.A. (2006). Heat generation and temperature prediction in metal cutting: A review and implications for high speed machining. International Journal of Machine Tools and Manufacture, 46(7–8), 782–800.

[36] Shet, C., Deng, X. (2000). Finite element analysis of the orthogonal metal cutting process. Journal of Materials Processing Technology, 105(1–2), 95–109.

[37] M'Saoubi, R., et al. (2008). A review of surface integrity in machining and its impact on functional performance and life of machined products. International Journal of Sustainable Manufacturing, 1(1–2), 203–236.

[38] Outeiro, J.C., Umbrello, D., M'Saoubi, R. (2006). Experimental and numerical modelling of the residual stresses induced in orthogonal cutting of AISI 316L steel. International Journal of Machine Tools and Manufacture, 46(14), 1786–1794.

[39] Brinksmeier, E., et al. (1999). Residual stresses—measurement and causes in machining processes. CIRP Annals, 31(2), 491–510.

[40] Filice, L., Micari, F., Settineri, L., Umbrello, D. (2007). Wear modelling in mild steel orthogonal cutting when using uncoated carbide tools. Wear, 262(5–6), 545–554.

[41] Attanasio, A., Ceretti, E., Giardini, C. (2008). Optimization of tool path in two points incremental forming. Journal of Materials Processing Technology, 177(1–3), 409–412.

[42] Brinksmeier, E., Gläbe, R., Schönemann, L. (2012). Review on diamond-machining processes for the generation of functional surface structures. CIRP Journal of Manufacturing Science and Technology, 5(1), 1–7.

[43] Ding, H., Shin, Y.C. (2012). A metallo-thermomechanically coupled analysis of orthogonal cutting of AISI 316L steel. Journal of Manufacturing Science and Engineering, 134(5), 051014.

[44] Hosford, W.F., Caddell, R.M. (2011). Metal Forming: Mechanics and Metallurgy, 4th Ed. Cambridge University Press.

[45] Keeler, S.P., Backofen, W.A. (1963). Plastic instability and fracture in sheets stretched over rigid punches. Trans. ASM, 56, 25–48.

[46] Barlat, F., Lege, D.J., Brem, J.C. (1991). A six-component yield function for anisotropic materials. International Journal of Plasticity, 7(7), 693–712.

[47] Maker, B.N., Zhu, X. (2000). Input parameters for metal forming simulation using LS-DYNA. Livermore Software Technology Corp., Technical Note.

[48] Schwarze, M., Reese, S. (2011). A reduced integration solid-shell finite element based on the EAS and the ANS concept—Large deformation problems. International Journal for Numerical Methods in Engineering, 85(3), 289–329.

[49] Emmens, W.C. (1997). Tribology of flat contacts and its application in deep drawing. PhD Thesis, University of Twente.

[50] Wanheim, T., Bay, N. (1978). A model for friction in metal forming processes. CIRP Annals, 27(1), 189–194.

[51] Nielsen, C.V., Martins, P.A.F. (2021). Metal Forming: Formability, Simulation, and Tool Design. Academic Press.

[52] Firat, M. (2007). Computer aided analysis and design of sheet metal forming processes: Part III—Stamping of a vehicle body panel. Materials and Design, 28(4), 1311–1320.

[53] Yoon, J.W., Barlat, F., Dick, R.E., Chung, K., Kang, T.J. (2000). Earing predictions based on asymmetric nonquadratic yield function. International Journal of Plasticity, 16(9), 1075–1104.

[54] Hiwatashi, S., Van Bael, A., Van Houtte, P., Teodosiu, C. (1998). Modelling of plastic anisotropy based on texture and dislocation structure. Computational Materials Science, 9(3–4), 274–284.

[55] Zhao, X., Gadreel, K., Gaul, L. (2017). Finite element simulation of deep drawing of 6061 aluminum alloy. Proc. ASME MSEC, Los Angeles, MSEC2017-2786.

[56] Gese, H., Oberhofer, G., Dell, H. (2009). Consistent modeling of plasticity and failure in the process chain from stamping to crash. Proc. LS-DYNA Forum, Bamberg.

[57] Abebe, M., Yoon, J.W. (2020). A review of wrinkling prediction and simulation in sheet metal forming processes. Journal of Materials Processing Technology, 283, 116662.

[58] Luo, L., Ghosh, A.K. (2003). Elastic and inelastic recovery after plastic deformation of DQSK steel sheet. Journal of Engineering Materials and Technology, 125(3), 237–246.

[59] Chaboche, J.L. (1989). Constitutive equations for cyclic plasticity and cyclic viscoplasticity. International Journal of Plasticity, 5(3), 247–302.

[60] Wagoner, R.H., Lim, H., Lee, M.G. (2013). Advanced issues in springback. International Journal of Plasticity, 45, 3–20.

[61] Yoshida, F., Uemori, T. (2002). A model of large-strain cyclic plasticity describing the Bauschinger effect and workhardening stagnation. International Journal of Plasticity, 18(5–6), 661–686.

[62] Barlat, F., Richmond, O. (1987). Prediction of tricomponent plane stress yield surfaces and associated flow and failure behavior of strongly textured FCC polycrystalline sheets. Materials Science and Engineering, 95, 15–29.

[63] Karafillis, A.P., Boyce, M.C. (1993). A general anisotropic yield criterion using bounds and a transformation weighting tensor. Journal of the Mechanics and Physics of Solids, 41(12), 1859–1886.

[64] Barlat, F., et al. (2005). Linear transfomation-based anisotropic yield functions. International Journal of Plasticity, 21(5), 1009–1039.

[65] Vegter, H., van den Boogaard, A.H. (2006). A plane stress yield function for anisotropic sheet material by interpolation of biaxial stress states. International Journal of Plasticity, 22(3), 557–580.

[66] Yoon, J.W., Barlat, F., Dick, R.E., Karabin, M.E. (2006). Prediction of six or eight ears in a drawn cup based on a new anisotropic theory. International Journal of Plasticity, 22(1), 174–193.

[67] Banabic, D., et al. (2010). Advanced Anisotropy Models and their Application in Sheet Metal Forming Simulation. IDDRG Conf. Proc., Graz.

[68] Cazacu, O., Barlat, F. (2001). Generalization of Drucker's yield criterion to orthotropy. Mathematics and Mechanics of Solids, 6(6), 613–630.

[69] Hutchinson, J.W., Neale, K.W. (1985). Wrinkling of curved thin sheet metal. In: Plastic Instability, 71–78, Presses ENPC.

[70] Correia, J.P.M., Ferron, G. (2002). Wrinkling of anisotropic metal sheets under deep drawing: analytical and numerical study. Journal of Materials Processing Technology, 128(1–3), 178–190.

[71] Marciniak, Z., Kuczyński, K. (1967). Limit strains in the processes of stretch-forming sheet metal. International Journal of Mechanical Sciences, 9(9), 609–620.

[72] Cao, J., Yao, H., Karafillis, A., Boyce, M.C. (2000). Prediction of localized thinning in sheet metal using a general anisotropic yield criterion. International Journal of Plasticity, 16(9), 1105–1129.

[73] Jawahir, I.S., Brinksmeier, E., M'Saoubi, R., Aspinwall, D.K. (2011). Surface integrity in material removal processes: Recent advances. CIRP Annals, 60(2), 603–626.

[74] Trigger, K.J., Chao, B.T. (1951). An analytical evaluation of metal cutting temperatures. Trans. ASME, 73, 57–68.

[75] Pan, B., Qian, K., Xie, H., Asundi, A. (2009). Two-dimensional digital image correlation for in-plane displacement and strain measurement: A review. Measurement Science and Technology, 20(6), 062001.

[76] Wagoner, R.H., Chenot, J.L. (2001). Metal Forming Analysis. Cambridge University Press.

[77] Sobol, I.M. (2001). Global sensitivity indices for nonlinear mathematical models and their Monte Carlo estimates. Mathematics and Computers in Simulation, 55(1–3), 271–280.

[78] Diehl, A., Engel, U., Geiger, M. (2010). Influence of microstructure on the mechanical properties and the

forming behaviour of very thin metal foils. International Journal of Advanced Manufacturing Technology, 47(1), 53–61.

[79] Roters, F., Eisenlohr, P., Hantcherli, L., Tjahjanto, D.D., Bieler, T.R., Raabe, D. (2010). Overview of constitutive laws, kinematics, homogenization and multiscale methods in crystal plasticity finite-element modeling: Theory, experiments, applications. Acta Materialia, 58(4), 1152–1211.

[80] Roters, F., Eisenlohr, P., Kords, C., Tjahjanto, D.D., Diehl, M., Raabe, D. (2012). DAMASK: The Düsseldorf Advanced MAterial Simulation Kit for studying crystal plasticity using an FE based or a spectral numerical solver. Proc. IUTAM, 3, 3–10.

[81] Geers, M.G.D., Kouznetsova, V.G., Brekelmans, W.A.M. (2010). Multi-scale computational homogenization: Trends and challenges. Journal of Computational and Applied Mathematics, 234(7), 2175–2182.

[82] Hornik, K., Stinchcombe, M., White, H. (1989). Multilayer feedforward networks are universal approximators. Neural Networks, 2(5), 359–366.

[83] Khalaj, G., Nazari, A., Pouraliakbar, H. (2013). Prediction of martensite fraction of microalloyed steel by artificial neural networks. Neural Computing and Applications, 22(3), 571–578.

[84] Raissi, M., Perdikaris, P., Karniadakis, G.E. (2019). Physics-informed neural networks: A deep learning framework for solving forward and inverse problems involving nonlinear partial differential equations. Journal of Computational Physics, 378, 686–707.

[85] Schulz, H. (1999). The history of high-speed machining. Revista de Ciência e Tecnologia, 7(13), 9–18.

[86] Lesuer, D.R., Kay, G.J., LeBlanc, M.M. (2001). Modeling large-strain, high-rate deformation in metals. Proc. 3rd Biennial Tri-Laboratory Engineering Conference, Albuquerque.

[87] Martins, P.A.F., Kwiatkowski, L., Franzen, V., Tekkaya, A.E., Kleiner, M. (2009). Single point incremental forming of polymers. CIRP Annals, 58(1), 229–232.

[88] Bambach, M., Taleb Araghi, B., Hirt, G. (2009). Strategies to improve the geometric accuracy in asymmetric single point incremental forming. Production Engineering, 3(2), 145–156.

[89] Grong, Ø., Shercliff, H.R. (2002). Microstructural modelling in metals processing. Progress in Materials Science, 47(2), 163–282.

[90] Shen, G., Shivpuri, R. (2006). A review of die life improvement from the perspective of die failure mechanisms in aluminum hot extrusion. Materials and Design, 27(10), 999–1010.